

Cite this: *Nanoscale*, 2012, **4**, 467

www.rsc.org/nanoscale

PAPER

# Conformationally pre-organized and pH-responsive flat dendrons: synthesis and self-assembly at the liquid–solid interface†

Tamer El Malah,<sup>‡a</sup> Artur Ciesielski,<sup>‡b</sup> Luc Piot,<sup>b</sup> Sergey I. Troyanov,<sup>c</sup> Uwe Mueller,<sup>d</sup> Steffen Weidner,<sup>e</sup> Paolo Samorì<sup>\*b</sup> and Stefan Hecht<sup>\*a</sup>

Received 2nd October 2011, Accepted 3rd November 2011

DOI: 10.1039/c1nr11434d

Efficient Cu-catalyzed 1,3-dipolar cycloaddition reactions have been used to prepare two series of three regioisomers of G-1 and G-2 poly(triazole-pyridine) dendrons. The G-1 and G-2 dendrons consist of branched yet conformationally pre-organized 2,6-bis(phenyl/pyridyl-1,2,3-triazol-4-yl)pyridine (BTP) monomeric and trimeric cores, respectively, carrying one focal and either two or four peripheral alkyl side chains. In the solid state, the conformation and supramolecular organization were studied by means of a single crystal X-ray structure analysis of one derivative. At the liquid–solid interface, the self-assembly behavior was investigated by scanning tunneling microscopy (STM) on graphite surfaces. Based on the observed supramolecular organization, it appears that the subtle balance between conformational preferences inherent in the dendritic backbone on the one side and the adsorption and packing of the alkyl side chains on the graphite substrate on the other side dictate the overall structure formation in 2D.

## Introduction

In recent years, the field of materials chemistry has greatly benefited from methodology development in organic synthesis.<sup>1</sup> In particular, the advent of “click chemistry”<sup>2</sup> has had a tremendous impact on synthetic macromolecular and supramolecular chemistry.<sup>3,4</sup> Although several reactions qualify as click chemistry,<sup>2</sup> it is most frequently associated with Cu-catalyzed Huisgen-type 1,3-dipolar cycloaddition reactions.<sup>5,6</sup> Due to the high yields that can be achieved in these linking reactions, click chemistry has been extensively exploited in materials chemistry over the past few years for the construction of a large variety of architectures, including linear polymers and block copolymers, hyperbranched polymers and dendrimers, macrocycles as well as catenanes and rotaxanes, among others.<sup>7</sup>

However, the connecting triazole moiety has thus far mostly served as a mere connecting unit.<sup>8</sup> To truly explore the potential of click chemistry, we have recently engaged in a program to utilize the formed triazole moiety as a key structural feature for the construction of various (macro)molecules with a defined shape.<sup>9</sup> In particular, the 2,6-bis(1-phenyl-1,2,3-triazol-4-yl)pyridine (BTP) motif<sup>9a</sup> was explored by us for the design of linear strands, *i.e.* helically folding oligomers<sup>9b</sup> and polymers,<sup>9c</sup> and linear tapes,<sup>9f</sup> and, most recently, to construct 2D folded, branched architectures, *i.e.* dendrimers.<sup>9g</sup> Due to lone pair repulsion, the extended *syn,syn* conformation of the BTP scaffold is strongly destabilized and hence the BTP has a high preference to adopt the “kinked” *anti,anti* conformation<sup>9a</sup> (Scheme 1), in analogy to the structurally related terpyridines.<sup>10</sup> In addition to providing a strong conformational preference, the BTP platform is responsive to the presence of protons or transition metal ions,<sup>9a,e</sup> a property that was used by us to prepare metallo-supramolecularly cross-linked gels<sup>9c</sup> and control the self-assembly of small BTP derivatives at the liquid–solid interface.<sup>9d</sup>

<sup>a</sup>Department of Chemistry, Humboldt-Universität zu Berlin, Brook-Taylor-Str. 2, 12489 Berlin, Germany. E-mail: sh@chemie.hu-berlin.de; Web: <http://www.hechtlab.de>

<sup>b</sup>ISIS/UMR CNRS 7006, Université de Strasbourg, 8 allée Gaspard Monge, 67000 Strasbourg, France. E-mail: samori@unistra.fr; Web: <http://www.nanochemistry.fr>

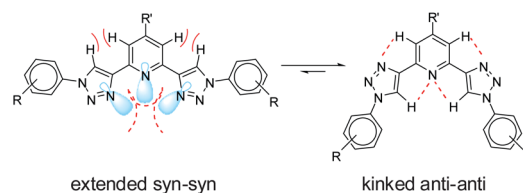
<sup>c</sup>Department of Chemistry, M. V. Lomonosov Moscow State University, 119991 Moscow, Russian Federation

<sup>d</sup>Helmholtz-Zentrum Berlin für Materialien und Energie GmbH, Elektronenspeicherung BESSY II, Albert-Einstein-Str. 15, 12489 Berlin, Germany

<sup>e</sup>Bundesanstalt für Materialforschung und -prüfung (BAM), Richard-Willstätter-Str. 11, 12489 Berlin, Germany

† Electronic supplementary information (ESI) available: Synthesis, experimental details, and characterization data. See DOI: 10.1039/c1nr11434d

‡ Both authors contributed equally to this work.



**Scheme 1** Conformational preference of the BTP scaffold to adopt a “kinked” *anti,anti* conformation mainly due to electrostatic and steric repulsions in the *syn,syn* conformation.

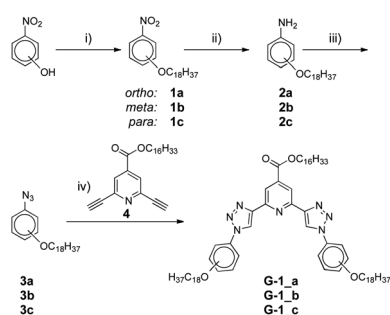
As evident from several crystal structures,<sup>9a,e,f</sup> the BTP core structure is highly conserved in its *anti,anti* conformation and resembles a flat heteroaromatic entity, which is able to stack very efficiently as reflected in the low solubility of unsubstituted derivatives. Based on these observations we became motivated to explore and extend from the BTP to the 2,6-bis(4-pyridyl-1,2,3-triazol-4-yl)pyridine (BTPP) motif for constructing heteroaromatic building blocks with a disc-like shape<sup>11</sup> to control their self-assembly in 2D on surfaces<sup>12</sup> as well as in 3D in bulk or in solution.<sup>13</sup> Here, we present the synthesis of three families of the first two generations of alkyl-substituted BTPP-based dendrons and the detailed investigation of their self-assembly behavior, in particular at the liquid–solid interface. Structural variation by regioisomeric attachment of alkyl side chains to the conformationally preorganized BTPP core enables control over self-assembly behavior in these novel electron-poor building blocks.

## Results and discussion

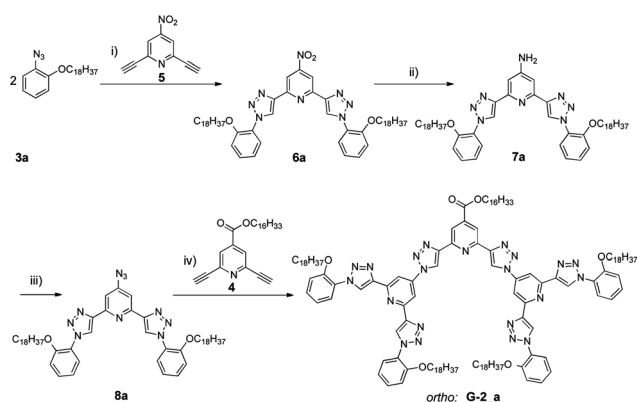
### Synthesis

To obtain the desired first generation G-1 derivatives, a modular and high yielding synthesis was developed based on the use of click-chemistry to merge the central hexadecylated pyridine building block **4**, readily available from citrazinic acid,<sup>9d</sup> with two terminal aromatic azides **3a–c** carrying long aliphatic side chains in the *ortho*-, *meta*-, or *para*-positions (Scheme 2). The azide termini **3a–c** were synthesized from the three different regioisomeric nitrophenols by an alkylation, reduction, diazotization sequence†. For the Cu-catalyzed 1,3-dipolar cycloaddition reaction a well established protocol<sup>5a</sup> was used, involving *in situ* formation of Cu(I) from CuSO<sub>4</sub> and sodium ascorbate as well as the addition of the tris[(1-benzyl-1*H*-1,2,3-triazol-4-yl)methyl]amine (TBTA) stabilizing ligand while working in a biphasic mixture of aqueous *tert*-butanol and methylene chloride. Target compounds **G-1\_a–c** were obtained in excellent yields and high purity after short column chromatography.

For the synthesis of higher generation dendrons a convergent-growth approach was initially explored (Scheme 3). For this purpose, two equivalents of 1-azido-2-(*n*-octadecyloxy)benzene **3a** were “clicked” to 2,6-diethynyl-4-nitropyridine **5** to yield **6a**,



**Scheme 2** Synthesis of first generation dendrons **G-1\_a–c**: (i) C<sub>18</sub>H<sub>37</sub>Br, K<sub>2</sub>CO<sub>3</sub>, 18-crown-6, TBAI, (CH<sub>3</sub>CN), 80 °C, **1a** (quant.), **1b** (96%), **1c** (98%); (ii) H<sub>2</sub>, Pd/C, (MeOH), 80 °C, **2a** (97%), **2b** (94%), **2c** (97%); (iii) (CH<sub>3</sub>)<sub>3</sub>CONO, TMSN<sub>3</sub>, (CH<sub>3</sub>CN), 0 °C, **3a** (69%), **3b** (64%), **3c** (70%); and (iv) CuSO<sub>4</sub>, TBTA, Na-asc., (H<sub>2</sub>O, *tert*-BuOH, CH<sub>2</sub>Cl<sub>2</sub>), 25 °C, **G-1\_a** (97%), **G-1\_b** (95%), **G-1\_c** (94%).



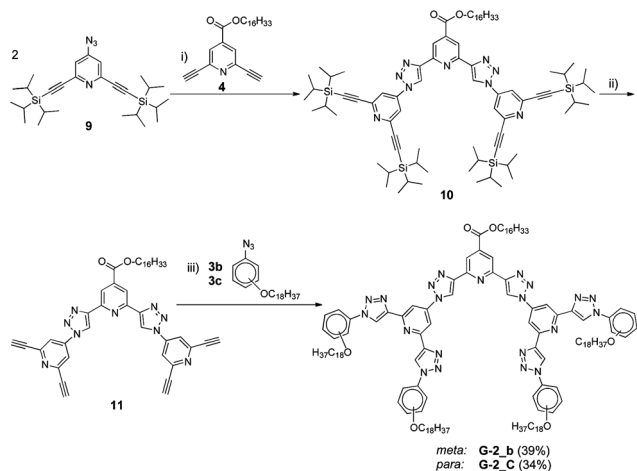
**Scheme 3** Convergent synthesis of second generation dendron *ortho* **G-2\_a**: (i) CuSO<sub>4</sub>, TBTA, Na-asc., (H<sub>2</sub>O, *tert*-BuOH, CH<sub>2</sub>Cl<sub>2</sub>), 25 °C, **6a** (65%); (ii) H<sub>2</sub>, Pd/C, (EtOAc), 25 °C, **7a** (98%); (iii) (CH<sub>3</sub>)<sub>3</sub>CONO, TMSN<sub>3</sub>, (CH<sub>3</sub>CN), 0 °C, **8a** (69%); and (iv) CuSO<sub>4</sub>, TBTA, Na-asc., (H<sub>2</sub>O, *tert*-BuOH, CH<sub>2</sub>Cl<sub>2</sub>), 25 °C, **G-2\_a** (43%).

which after activation by a reduction/diazotization sequence yielded G-1 dendron **8a** carrying a focal azide functionality, ready to engage in another two-fold click reaction with pyridine **4** to yield the desired second generation dendron **G-2\_a**. Note that introduction of the peripheral alkoxy substituents already occurs at the intermediate first generation stage.

An alternative divergent route was utilized to prepare the regioisomeric second generation dendrons **G2\_b** and **G-2\_c** (Scheme 4). Here, two equivalents of the AB'<sub>2</sub> monomer **9** are coupled to core molecule **4**, yielding tetra-silyl-protected second generation dendron **10**, which is functionalized at its periphery by desilylation followed by cycloaddition with the appropriate azide to give the other two regioisomeric second generation dendrons **G-2\_b** and **G-2\_c**.

### Single crystal X-ray diffraction

In the case of **G-1\_a**, single crystals could be grown from acetone suitable for X-ray structural analysis. **G-1\_a** crystallizes in



**Scheme 4** Divergent synthesis of second generation **G-2\_b,c** *meta*- and *para*-derivatives: (i) CuSO<sub>4</sub>, TBTA, Na-asc., (H<sub>2</sub>O, *tert*-BuOH, CH<sub>2</sub>Cl<sub>2</sub>), 25 °C, **10** (61%); (ii) TBAF, (THF), 0 °C, **11** (98%); and (iii) CuSO<sub>4</sub>, TBTA, Na-asc., (H<sub>2</sub>O, *tert*-BuOH, CH<sub>2</sub>Cl<sub>2</sub>), 25 °C, **G-2\_b** (39%), **G-2\_c** (34%).

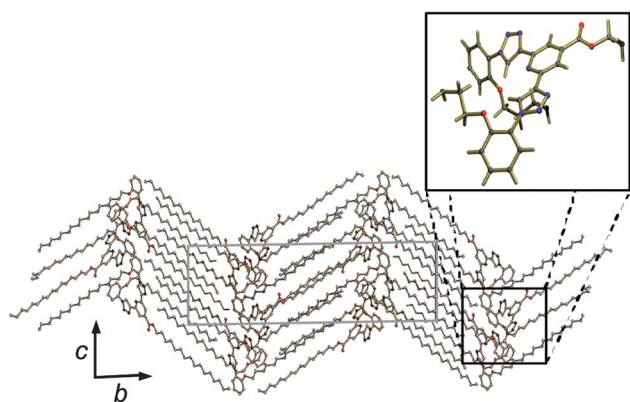


**Fig. 1** Molecular packing of **G-1\_a** within a single crystal showing a lamellar structure (viewed along the direction). The inset shows a zoom of the BTP core to illustrate its conformational preferences for the “kinked” *anti,anti* conformation and the interactions of the O atoms of the *ortho*-alkoxy groups (H atoms are omitted for clarity).

a rather simple space group presenting an inversion center, requiring thus the translation of only two molecules to generate the whole structure. The structure consists of columnar organized heteroaromatic BTP cores, which are separated by lamellar segments composed of the alkyl side chains (Fig. 1).

Closer inspection of the structure reveals that the BTP cores adopt a preferred conformation not only with regard to the pyridine–triazole connections (*anti,anti* conformation) but also with regard to their phenyl–triazole bonds. Lone pair repulsion between the *ortho*-ether substituent and the triazole nitrogen (N-2) on the one hand and favorable electrostatic interactions between the *ortho*-phenyl proton (H-2) and the triazole nitrogen (N-2) on the other hand favor an *anti* conformation at both phenyl–triazole ring junctions. This conformational restriction dictates the projection of the long alkyl chains at the observed angle, giving rise to an overall “zig-zag” structure. It appears that maximizing van der Waals contacts between the *all-trans* alkyl chains is the dominating driving force for structure formation as  $\pi, \pi$ -stacking is restricted within the helical BTP columns and distances of 5 Å indicate rather weak interactions, which might however be attenuated by their dipolar character. Therefore, the decisive role of the BTP core is most likely the arrangement of the side chains in space, which largely depends on both conformational preferences of the BTP backbone as well as the sites of side chain attachment, *i.e.* regiochemistry.

### Self-assembly at the solid–liquid interface

To gain further insight into the self-assembly of BTP and BTP derivatives, we extended our studies to STM investigations at the solid–liquid interface, with the aim of elucidating the tendency to form 2D crystalline monolayers of the different BTPs and BTPs when physisorbed on highly oriented pyrolytic graphite (HOPG) surfaces. First, STM imaging was performed on a monolayer of **G-1\_a**, prepared by applying a drop of a diluted solution in 1-phenyloctane onto HOPG. The large-scale image (Fig. 2a) exhibits extended arrays with long range order reflecting a rosette-like structure. In the high resolution STM image (Fig. 2b), it is possible to identify individual physisorbed

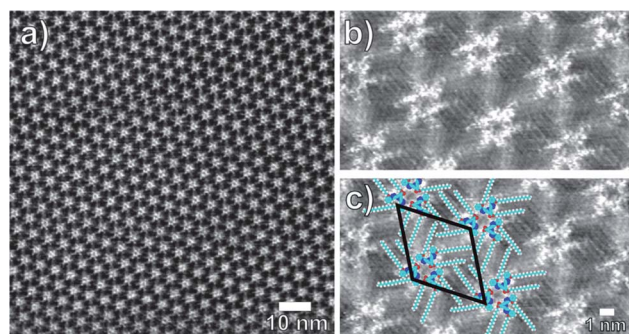


**Fig. 2** (a) Monolayer of **G-1\_a** on HOPG displaying a “rosette” motif. (b and c) Zoom-in and proposed molecular packing model showing the BTP-a molecules in their “kinked” *anti,anti* conformation (unit-cell parameters:  $a = 5.1 \pm 0.2$  nm,  $b = 5.0 \pm 0.2$  nm,  $\gamma = 61 \pm 2^\circ$ ,  $A \text{ mol}^{-1} = 7.4 \pm 1.1$  nm<sup>2</sup>; tunneling parameters: bias voltage  $U_t = 800$  mV, average tunneling current  $I_t = 5$  pA.).

molecules and their different functionalities. In fact the contrast in STM images of alkyl substituted molecules incorporating a  $\pi$ -conjugated backbone or core is ruled by resonant tunneling between the Fermi level of the HOPG and the frontier orbitals of the adsorbed molecules.<sup>14</sup> The bright spots can thus be ascribed to the BTP aromatic cores, whereas the darkest linear features correspond to the aliphatic residues. From the proposed model (Fig. 2c) it clearly appears that each “rosette” motif is composed of trimers of **G-1\_a** molecules with all their alkoxy chains adsorbed on the surface surrounding the aromatic cores. Noteworthy in the nanopattern obtained with the *ortho*-substituted **G-1\_a** molecules, the alkyl side chains adopt a fully extended conformation and are oriented according to the three-fold symmetry of the HOPG substrate. This is achieved by maintaining the kinked *anti,anti* conformation, which is thermodynamically preferred in solution.<sup>9a</sup> However, in contrast to the solid state structure of **G-1\_a** (Fig. 1), one terminal phenyl ring is rotated about the bond connecting it to the adjacent triazole moiety, thereby enabling projection of the attached side chain in the same direction as the central side chain. By assembly of three of these pie-shaped wedges into a circular rosette with a three-fold symmetry, matching of the alkyl chain periodicity with the underlying substrate can be realized.

In the case of **G-1\_b**, the observed self-assembled lamellar pattern (Fig. 3) is markedly different from the motif as observed for **G-1\_b**. At first sight, nanoscale phase segregation between the conjugated and the aliphatic parts of the molecules becomes

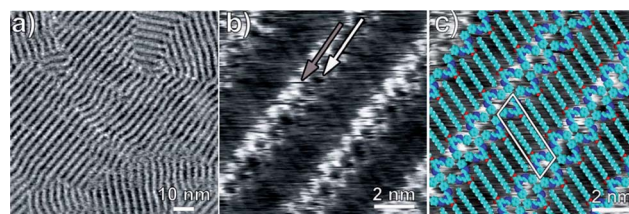


**Fig. 3** (a) STM images of the lamellar assemblies of **G-1\_b** physisorbed on HOPG. (b and c) Zoom-in and proposed molecular packing model showing the **G-1\_b** molecules in their “extended” *syn,syn* conformation (unit-cell parameters:  $a = 1.3 \pm 0.2$  nm,  $b = 3.6 \pm 0.2$  nm,  $\gamma = 70 \pm 2^\circ$ ,  $A = 4.5 \pm 0.4$  nm<sup>2</sup>; tunneling parameters:  $U_t = 500$  mV,  $I_t = 20$  pA).

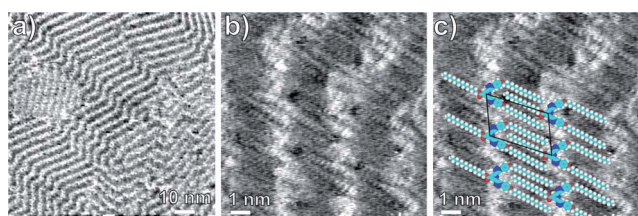


**Fig. 4** (a) STM images of the lamellar assemblies of **G-1\_c** physisorbed on HOPG. (b and c) Zoom-in and proposed molecular packing model showing the **G-1\_c** molecules in their “kinked” *anti,anti* conformation (unit-cell parameters:  $a = 2.1 \pm 0.2$  nm,  $b = 3.3 \pm 0.2$  nm,  $\gamma = 68 \pm 2^\circ$ ,  $A$  mol<sup>-1</sup> =  $6.4 \pm 1.0$  nm<sup>2</sup>; tunneling parameters:  $U_t = 500$  mV,  $I_t = 5$  pA).

apparent. The **G-1\_b** monolayer shows a lower degree of crystallinity as evidenced by the size of the crystalline domains not exceeding a few tens of nanometres and by the presence of numerous defects in the lamellar structure (Fig. 3a). High resolution STM imaging (Fig. 3b) reveals the sub-molecularly resolved structure of the pattern: brighter linear parts, which can be ascribed to the aromatic cores, are surrounded by the interdigitated alkoxy chains that appear darker. Each lamellar structure consists of two rows of **G-1\_b** molecules. The two adjacent rows of the BTP cores (indicated with white and gray arrows) exhibit a different contrast. This can be ascribed to the different geometrical overlap of the frontier orbitals of the adsorbate molecules with the lattice of HOPG. The BTP cores adopt the favored *anti,anti* conformation. The loosely packed nature of the architecture in the dark area of the STM image, *i.e.* the region containing the alkyl chains, determines a limited stability of the 2D-structure, which is reflected in the limited size of the crystalline domains (Fig. 3a). It is worth noting that two *meta*-substituted side chains of each molecule are back-folded in the supernatant solution, a behavior previously observed for other systems exposing alkoxy side chains.<sup>15</sup>

STM imaging of a **G-1\_c** monolayer (Fig. 4a) reveals a polycrystalline structure consisting of lamellae. As in the case of **G-1\_b**, the monolayer shows numerous defects and rather small domain sizes. The intrinsic conformation adopted by the BTP cores is identical to the two previous cases as observed in the high resolution STM images (Fig. 4b and c). **G-1\_c** molecules adopt the “kinked” *anti,anti* conformation with all their alkyl residues adsorbed on the surface and interdigitated with side chains of molecules belonging to neighboring lamellae. This leads to a more loose packing in agreement with the increased area of the unit cell.

The STM investigations nicely show that subtle differences in the substitution pattern of the regioisomeric **G-1\_a-c** lead to pronounced effects of their 2D self-assembly at the liquid–solid interface. These marked differences are primarily caused by the energetic interplay between the conformational preferences of the BTP core in combination with the ability to arrange the appended alkyl side chains in a dense packing commensurate with the underlying HOPG substrate. Noteworthily, co-adsorption of the solvent molecules, *i.e.* 1-phenyloctane, can be neglected, as confirmed by the tight packing of the molecules on the basal plane of the graphite surface.

Our investigations were extended to the second generation dendrons. STM images of a monolayer of **G-2\_b** (Fig. 5a) and **G-**

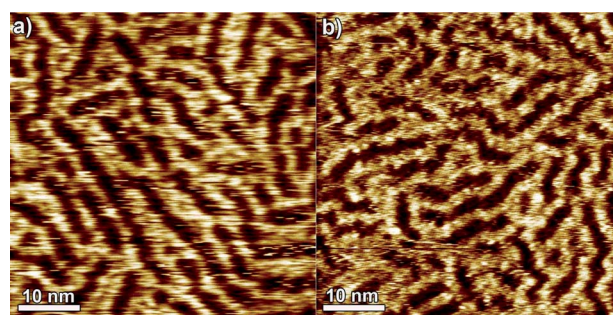


**Fig. 5** STM image of the “disordered” assembly of (a) **G-2\_b** and (b) **G-2\_c** physisorbed on HOPG; tunneling parameters:  $U_t = 500$  mV,  $I_t = 5$  pA.

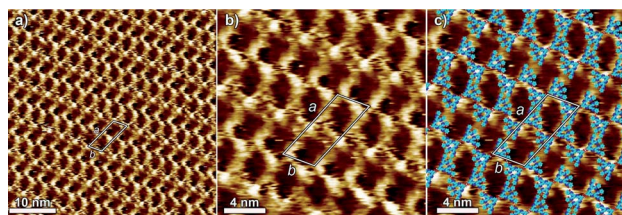
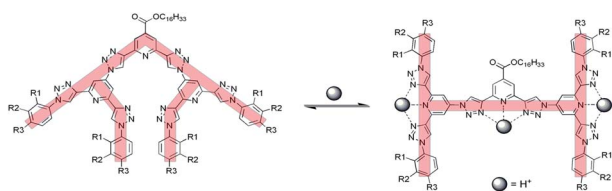


**Fig. 6** STM image of the lamellar assembly of **G-2\_a** physisorbed on HOPG. (b and c) Zoom-in and proposed molecular packing model showing the **G-2\_a** molecules in their “kinked” *anti,anti-anti,anti* conformation (unit-cell parameters:  $a = 7.9 \pm 0.2$  nm,  $b = 3.1 \pm 0.2$  nm,  $\gamma = 68 \pm 2^\circ$ ,  $A = 22.7 \pm 1.5$  nm<sup>2</sup>; tunneling parameters:  $U_t = 500$  mV,  $I_t = 5$  pA).

**2\_c** (Fig. 5b), prepared by applying a drop of a diluted solution in 1,2,4-trichlorobenzene (TCB) onto HOPG, show formation of nanophase-separated yet disordered 2D-structures on the graphite surface.

In strong contrast, applying a drop of a diluted solution of **G-2\_a** in TCB onto a HOPG surface, well-ordered monolayers were observed (Fig. 6). The proposed structural model (Fig. 6c) suggests that each unit cell is composed of four **G-2\_a** molecules, which are probably interacting *via* van der Waals forces. It is likely that all *ortho*-substituted side chains are physisorbed on the HOPG surface, although, presumably owing to their highly dynamic nature on the time scale of the STM imaging, we are unable to resolve them. It is important to note that all **G-2** molecules were visualized only at the solution–graphite interface using TCB as solvent. Study of these systems in different solvents, *i.e.* 1-phenyloctane or tetradecane, did not produce any ordered monolayer formation. Since the **G-2\_a** molecules are not tightly packed as in the case of the first generation of dendrons, co-adsorption of TCB molecules is possible. However, the mobility of the TCB molecules at surfaces is faster than the time scale of the STM imaging, thus hindering the visualization of the TCB molecule by STM.

In order to trigger the switching of the **G-2** molecules from the “kinked” to the “extended” conformation (Scheme 5), a small amount of trifluoroacetic acid (1 mM TFA in TCB) was added on top of the solution covering the already formed monolayers on the surface. Noteworthily, conformational switching of the **G-1** molecules upon acidification and/or metallation of existing monolayers has been discussed elsewhere.<sup>9d</sup>



**Scheme 5** Proton-triggered structural change of the **G-2** molecules from their “kinked” to their “extended” conformation.

Surprisingly, only one out of three **G-2** derivatives was found to undergo conformational changes upon *in situ* acidification of existing monolayers. The physisorbed monolayer of **G-2<sub>b</sub>** obtained after applying the acidified solution (5  $\mu\text{L}$  of 1 mM solution of TFA in TCB) to the surface displays a 2D architecture consisting of a lamellar-like motif, which appeared on the surface 60 seconds after the deposition of the acidified solution (Fig. 7). The lamellar domains extend over tens of nanometres and no part of the substrate surface was found to be occupied by molecules adsorbed in the previously described “disordered” packing (see Fig. 5a). The high resolution image (Fig. 7b) reveals that the adsorbed molecules adopt an “extended” conformation as sketched in Scheme 5, thereby unequivocally confirming the occurrence of protonation. It is likely that all *meta*-substituted side chains are back-folded into the supernatant solution, and the cavities formed upon reorganization of assembly occupied by TCB molecules. However taking into account their highly dynamic nature, it is not possible to visualize them by STM. The proposed packing model (Fig. 7c), extrapolated from high resolution STM measurements, shows convincingly that the **G-2<sub>b</sub>** cores adopt an “extended” conformation, in line with protonation. Significantly, virtually identical protonation-driven transformations were observed both for *ex situ* and *in situ* acidifications of **G-2<sub>b</sub>** molecules.

The conformational switch and the corresponding reorganization of the self-assembled pattern occurring at the solid–liquid interface have been monitored *in situ* on the length scale of several tens of nanometres (Fig. 8). The transformation from the disordered layer to the “lamellar” motif for **G-2<sub>b</sub>** based monolayers could furthermore be monitored in real-time on the time scale of several tens of seconds, taking advantage of the slow nature of the reorganization process. The observed slow switching kinetics are caused by the long alkoxy chains of **G-2<sub>b</sub>**, providing an increased desorption energy on graphite and hence a partial hindrance towards reorganization of the self-assembled

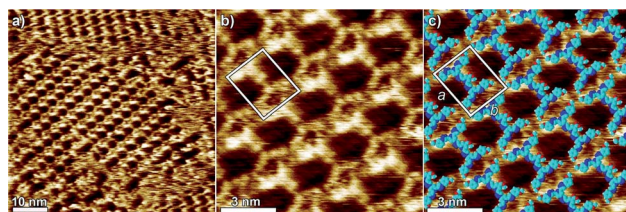


**Fig. 7** STM image of the lamellar assembly of **G-2<sub>b</sub>** physisorbed on HOPG. (b and c) Zoom-in and proposed molecular packing model showing the **G-2<sub>b</sub>** molecules in their “extended” conformation (unit-cell parameters:  $a = 3.2 \pm 0.2$  nm,  $b = 2.6 \pm 0.2$  nm,  $\gamma = 93 \pm 2^\circ$ ,  $A = 8.3 \pm 0.6$  nm<sup>2</sup>; tunneling parameters:  $U_t = 500$  mV,  $I_t = 5$  pA).

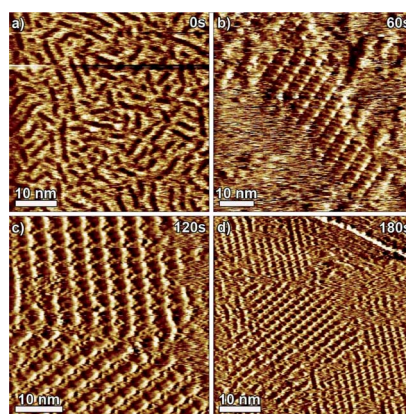


**Fig. 8** Consecutive STM images showing the structural evolution of a monolayer of **G-2<sub>b</sub>** over 3 min after the addition of *ca.* 5  $\mu\text{L}$  of 1 mM solution of TFA in TCB. (a) Image taken right before the addition of TFA, (b) after 1 min, (c) after 2 min, and (d) after 3 min. The unit cell found for the new packing corresponds exactly to the one of the tetragon structure (tunneling parameters:  $U_t = 500$  mV,  $I_t = 10$  pA).

motif.<sup>9d</sup> A set of measurements, in which the “disordered” layer is gradually converted into a “lamellar” one over the time scale of 20 min (Fig. 8), shows that the “lamellar” packing becomes the more favorable over time. The total coverage of the surface by the “lamellae” assembly is completed a few minutes after the deposition of the droplet of the acidified solution. The fuzzy parts on the STM images most likely correspond to areas where the considerable mobility of the molecules, triggered by the protonation process, hinders high resolution STM imaging.

Interestingly, only one out of three **G-2** derivatives, *i.e.* **G-2<sub>b</sub>**, was found to undergo conformational changes upon acidification. In the case of **G-2<sub>a</sub>**, this may be ascribed to the need for disassembly of an extended 2D packing (Fig. 6) to achieve structural re-organization as a result of molecular complexation with proton(s). In the case of **G-2<sub>a</sub>** and **G-2<sub>c</sub>** an important role may be played by the steric hindrance between alkoxy substituents. However STM imaging at the solid–liquid interface cannot offer real-time monitoring of the reaction process in its intermediate states, thus the role of the alkoxy substituents of **G-2<sub>a</sub>** and **G-2<sub>c</sub>** cannot be unambiguously determined.

## Conclusions

First and second generations of shape-persistent dendrons, equipped with long alkyl chains needed to provide solubility and facilitate self-assembly on graphite substrates, were readily synthesized by click chemistry. Detailed structural insight into the bulk could be obtained by X-ray diffraction on single crystals of the first generation dendron **G-1<sub>a</sub>**, showing lamellae formation of strongly intercalated alkyl side chains and columnar organization of the BTP and BPTP cores. Confining aggregation of these **G-1** and **G-2** derivatives to two dimensions at the liquid–solid interface gave rise to formation of self-assembled monolayers on graphite surfaces. High resolution scanning tunneling microscopy revealed markedly different packing motifs due to both different conformations adopted by the BTP and BPTP cores as well as the dominating adsorption and crystallization of the aliphatic chains.

In both 2D and 3D aggregations, there is a subtle balance between the conformational preference of the BTP and BPTP cores for adopting the “kinked” *anti,anti* conformation and the ability of the alkyl chains to organize into a closely packed arrangement to maximize van der Waals interactions. The point of attachment of the alkyl chains to the BTP/BPTP termini, *i.e.* *ortho-* vs. *meta-* vs. *para-*substitution, dictates if the BTP/BPTP derivative is able to optimize packing in 2D or 3D. The observed dependence of aggregation behavior on core conformation and attachment of alkyl side chains is of general importance for the self-assembly of electron-deficient (hetero)aromatic moieties,<sup>16</sup> necessary to achieve electron-transporting materials with reasonable mobilities to be used in organic electronic devices.<sup>17</sup> Furthermore, the unique ability of some of our first and second generation dendrons to adopt quite different adsorption conformations and hence self-assembly structures allows for the generation of chemo-responsive nanopatterns.

## Acknowledgements

This work was supported by the ERA-Chemistry project Sur-ConFold, the EU through the projects ITN-SUPERIOR (PITN-GA-2009-238177) and FP7 ONE-P large-scale project no. 212311, the NanoSci-E+ project SENSORS, the International Center for Frontier Research in Chemistry (FRC, Strasbourg) and the Fonds der Chemischen Industrie. T.E.M. is grateful to the Egyptian government for providing a doctoral fellowship. The authors thank Wacker AG, BASF AG, Bayer Industry Services, and Sasol Germany for generous donations of chemicals.

## References

- (a) C. J. Hawker and K. L. Wooley, *Science*, 2005, **309**, 1200; (b) S. Hecht, *Mater. Today*, 2005, **8**, 48.
- The concept of “click-chemistry” is described in: C. Kolb, M. G. Finn and K. B. Sharpless, *Angew. Chem., Int. Ed.*, 2001, **40**, 2004.
- For reviews about the application of “click-chemistry” in polymer and materials science, see: (a) J.-F. Lutz, *Angew. Chem., Int. Ed.*, 2007, **46**, 1018; (b) W. H. Binder and R. Sachsenhofer, *Macromol. Rapid Commun.*, 2007, **28**, 15; (c) D. Fournier, R. Hoogenboom and U. S. Schubert, *Chem. Soc. Rev.*, 2007, **36**, 1369.
- Prominent examples include: (a) dendrimer synthesis: P. Wu, A. K. Feldman, A. K. Nugent, C. J. Hawker, A. Scheel, B. Voit, J. Pyun, J. M. J. Fréchet, K. B. Sharpless and V. V. Fokin, *Angew. Chem., Int. Ed.*, 2004, **43**, 3928; (b) dendronization of linear polymers: B. Helms, J. L. Mynar, C. J. Hawker and J. M. J. Fréchet, *J. Am. Chem. Soc.*, 2004, **126**, 15020; (c) postfunctionalization of linear polymers: P. L. Golas, N. V. Tsarevsky, B. S. Sumerlin and K. Matyjaszewski, *Macromolecules*, 2006, **39**, 6451; (d) postfunctionalization of helical foldamers: H. J. Kitto, E. Schwartz, M. Nijemeisland, M. Koepf, J. J. L. M. Cornelissen, A. E. Rowan and R. J. M. Nolte, *J. Mater. Chem.*, 2008, **18**, 5615; (e) crosslinked polymer glue: D. D. Díaz, S. Punna, P. Holzer, A. K. McPherson, K. B. Sharpless, V. V. Fokin and M. G. Finn, *J. Polym. Sci., Part A: Polym. Chem.*, 2004, **42**, 4392; (f) stabilization of organogels: D. D. Díaz, K. Rajgopal, E. Strable, J. Schneider and M. G. Finn, *J. Am. Chem. Soc.*, 2006, **128**, 6056; (g) functionalization of single-walled

- carbon nanotubes: H. Li, F. Cheng, A. M. Duft and A. Adronov, *J. Am. Chem. Soc.*, 2005, **127**, 14518.
- Original work: (a) V. V. Rostovtsev, L. G. Green, V. V. Fokin and K. B. Sharpless, *Angew. Chem., Int. Ed.*, 2002, **41**, 2596; (b) C. W. Tornøe, C. Christensen and M. Meldal, *J. Org. Chem.*, 2002, **67**, 3057, please note that the non-catalyzed, thermal [4 + 2] cycloaddition reactions of various 1,3-dipoles have been pioneered by Huisgen, see: (c) R. Huisgen, in *1,3-Dipolar Cycloaddition Chemistry*, ed. A. Padwa, Wiley, New York, 1984, p. 1.
  - In addition, in particular the radical addition of thiols to olefins, the so called thiol-ene reaction, has been widely used recently: (a) K. L. Killos, L. M. Campos and C. J. Hawker, *J. Am. Chem. Soc.*, 2008, **130**, 5062; (b) V. S. Khire, Y. Yi, N. A. Clark and C. N. Bowman, *Adv. Mater.*, 2008, **20**, 3308; (c) L. M. Campose, I. Meinel, R. G. Guino, M. Schierhorn, N. Gupta, G. D. Stucky and C. J. Hawker, *Adv. Mater.*, 2008, **20**, 3728.
  - For a general review see: M. Meldal and C. W. Tornøe, *Chem. Rev.*, 2008, **108**, 2952 and references therein.
  - Notable exceptions are triazole isosteres in pseudopeptides: L. Angell and K. Burgess, *Chem. Soc. Rev.*, 2007, **36**, 1674.
  - (a) R. M. Meudtner, M. Ostermeier, R. Goddard, C. Limberg and S. Hecht, *Chem.–Eur. J.*, 2007, **13**, 9834; (b) R. M. Meudtner and S. Hecht, *Angew. Chem., Int. Ed.*, 2008, **47**, 4926; (c) R. M. Meudtner and S. Hecht, *Macromol. Rapid Commun.*, 2008, **29**, 347; (d) L. Piot, R. M. Meudtner, T. El Malah, S. Hecht and P. Samorì, *Chem.–Eur. J.*, 2009, **15**, 4788; (e) M. Ostermeier, M.-A. Berlin, R. Meudtner, S. Demeshko, F. Meyer, C. Limberg and S. Hecht, *Chem.–Eur. J.*, 2010, **16**, 10202; (f) D. Zornik, R. M. Meudtner, T. El Malah, C. M. Thiele and S. Hecht, *Chem.–Eur. J.*, 2011, **17**, 1473; (g) A. Cadeddu, A. Ciesielski, T. El Malah, S. Hecht and P. Samorì, *Chem. Commun.*, 2011, **47**, 10578.
  - U. S. Schubert, H. Hofmeier and G. R. Newkome, *Modern Terpyridine Chemistry*, Wiley-VCH, Weinheim, 2006.
  - For a notable exception of a flat heteroaromatic disc-shaped system planarized by H-bonding see: L. Brunsveld, H. Zhang, M. Glasbeek, J. A. J. M. Vekemans and E. W. Meijer, *J. Am. Chem. Soc.*, 2000, **122**, 6175.
  - For a review see: (a) A. W. Bosman, H. M. Janssen and E. W. Meijer, *Chem. Rev.*, 1999, **99**, 1665, for selected examples see; (b) S. Uemura, S. Sengupta and F. Würthner, *Angew. Chem., Int. Ed.*, 2008, **48**, 7825; (c) S. D. Hudson, H.-T. Jung, V. Percec, W.-D. Cho, G. Johansson, G. Ungar and V. S. K. Balagurusamy, *Science*, 1997, **278**, 449; (d) B. Dong, F. Huo, L. Zhang, X. Yang, Z. Wang, X. Zhang, S. Gong and J. Li, *Chem.–Eur. J.*, 2003, **9**, 2331; (e) P. Wu, Q. Fan, Q. Zeng, C. Wang, G. Deng and C. Bai, *ChemPhysChem*, 2002, **7**, 633; (f) L. Merz, H.-J. Güntherodt, L. J. Scherer, E. C. Constable, C. E. Housecroft, M. Neuburger and B. A. Hermann, *Chem.–Eur. J.*, 2005, **11**, 2307.
  - For prominent reviews see: (a) F. Zeng and S. C. Zimmerman, *Chem. Rev.*, 1997, **97**, 1681; (b) B. M. Rosen, C. J. Wilson, D. A. Wilson, M. Peterca, M. R. Imam and V. Percec, *Chem. Rev.*, 2009, **109**, 6275; and ref. 12a.
  - R. Lazzaroni, A. Calderone, J.-L. Brédas and J. P. Rabe, *J. Chem. Phys.*, 1997, **107**, 99.
  - (a) S. B. Lei, K. Tahara, F. C. de Schryver, M. van der Auweraer, Y. Tobe and S. De Feyter, *Angew. Chem., Int. Ed.*, 2008, **47**, 2964; (b) Y. Kaneda, M. E. Stawasz, D. L. Sampson and B. A. Parkinson, *Langmuir*, 2001, **17**, 6185.
  - For a prominent review see: F. J. M. Hoeben, P. Jonkheijm, E. W. Meijer and A. P. H. J. Schenning, *Chem. Rev.*, 2005, **105**, 1491.
  - For selected recent examples, see: (a) H. N. Tsao, W. Pisula, Z. H. Liu, W. Osikowicz, W. R. Salaneck and K. Müllen, *Adv. Mater.*, 2008, **20**, 2715; (b) R. Schmidt, J. H. Oh, Y. S. Sun, M. Deppisch, A. M. Krause, K. Radacki, H. Braunschweig, M. Konemann, P. Erk, Z. A. Bao and F. Würthner, *J. Am. Chem. Soc.*, 2009, **131**, 6215; (c) H. Yan, Z. H. Chen, Y. Zheng, C. Newman, J. R. Quinn, F. Dotz, M. Kastler and A. Facchetti, *Nature*, 2009, **457**, 679.